# Theoretical Study of the Thermal Decomposition of *N,N′*-Diacyl-*N,N′*-Dialkoxyhydrazines: A Comparison of HF, MP2, and DFT

**Lisa M. Thomson and Michael B. Hall***

*Department of Chemistry, Texas A&M University, College Station, Texas 77843*

*Received: February 17, 2000; In Final Form: April 19, 2000*

The thermal decomposition of *N,N′*-diacyl-*N,N′*-dialkoxyhydrazines, $(N(COR^1)(OR^2))_2$, to the corresponding ester and dinitrogen was investigated with high-level ab initio and density functional calculations. The results suggest that the decomposition proceeds via a two step 1,1-elimination. Coupled cluster calculations on several model systems ($R^1{=}R^2{=}H$; $R^1{=}CH_3$, $R^2{=}H$; $R^1{=}R^2{=}CH_3$) at the density functional geometry (CCSD(T)// B3P86) with zero-point energy and thermal corrections at the B3P86 level show that the barrier for the first elimination, the rate-determining step, is 24−34 kcal/mol, while the barrier for the second step in the two step 1,1-elimination is only 1−3 kcal/mol, a value that is much smaller than the exothermicity of the first step. This result explains why experimentalists have been unable to trap the intermediate nitrene. The critical point associated with the concerted elimination is shown to be a second-order saddle point on the potential energy surface at the HF and density functional levels of theory with energies of 139.2 and 88.4 kcal/mol above the reactant, respectively. An unexpected result of this study was the failure of Hartree−Fock (HF) and Møller−Plesset second order perturbation (MP2) to properly describe every aspect of this seemingly simple system.

## Introduction

Experimental work[1] has shown that the thermal decomposition of *N,N′*-diacyl-*N,N′*-dialkoxyhydrazines **1** is a potential source of sensitive highly hindered esters, **6**, and olefins.[2] It has also been shown that the preparation of benzyne from 1-*N*-aminobenzotriazole invloves the elimination of two molecules of nitrogen.[2] The quantitative synthesis of **1** can be achieved by the oxidation of *o*-alkyl-hydroxymates ($R^1CONHOR^2$) with nickel peroxide ($NiO_2{\cdot}H_2O$) or ceric ammonium nitrate (CAN) under mild conditions (−20−25 °C/3−32 h) for a variety of R groups including keto-methoxime, benzoyl, aryl, and alkyl substituents.[1] The resulting hydrazine **1** can then be decomposed under mild conditions (25−160 °C/0.5−12 h) to afford dinitrogen, **5**, and the corresponding ester, **6**, in high yields (87−100%). See Scheme 1. Three mechanisms (Scheme 2) have been proposed for the decomposition of **1**. Pathway I is a one-step concerted elimination of the esters, **6**. Pathway II is a two-step 1,2-elimination of the ester, **6**, via an azo intermediate. Pathway III is a two-step 1,1-elimination of the ester, **6**, via a singlet or triplet nitrene intermediate. Pathway II was originally proposed as the mechanism for the decomposition of **1** based on kinetic measurements.[3] Recently, II has been investigated experimentally[1] by studying the decomposition of an unsymmetrical hydrazine prepared with $R^1$=cyclohexyl, $R^2$=methyl, $R^{1'}$=benzyl, and $R^{2'}$=phenethyl. Two products were formed quantitatively in a 1:1 ratio: methyl cyclohexylcarboxylate and benzyl 3-phenylpropanoate. These results excluded the possibility of pathway II but the question remained as to whether the decomposition occurred via a concerted path (I) or a two step 1,1-elimination (III).

Previous theoretical work[1] has also been performed on the decomposition of **1**. These calculations were at the semiempirical level[4] and indicated that the concerted elimination (I) was less favorable by 51.7 kcal/mol than the two-step 1,1-elimination (III). This result is consistent with the fact that in two point groups ($C_i$ and $C_s$) the concerted elimination is symmetry forbidden, while only along a $C_2$ (or $C_1$) pathway is it symmetry allowed. Experiments have been designed to capture any intermediate nitrenes with cyclohexene, styrene, DMSO, nitrosobenzene, DEAD, and dimethyl fumarate, which would prove that pathway III is followed, but they have been unsuccessful. The semiempirical results indicated that the second barrier for the 1,1-elimination was lower in energy than the exothermicity of the first step; thus, it might be difficult to capture the intermediate nitrene. The semiempirical results gave a qualitative description of the reaction but the absolute magnitudes are not accurate.

**SCHEME 1**

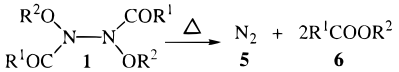

system **a** $R^1{=}R^2{=}H$
system **b** $R^1{=}CH_3$ $R^2{=}H$
system **c** $R^1{=}R^2{=}CH_3$

**SCHEME 2**

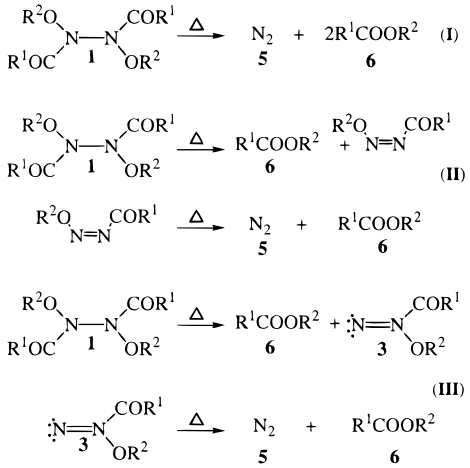

10.1021/jp000623z CCC: $19.00 
Published on Web 06/10/2000

In this study, high-level density functional and ab initio calculations will be performed on all of the species involved in pathways I and III to (1) examine the conclusion drawn from the semiempirical results; (2) compare HF, MP2, and DFT; and (3) give a quantitative description of the reaction mechanism involved in the thermal decomposition of **1**. A detailed description of the thermal decomposition of *N*,*N*′-diacyl-*N*,*N*′-dialkoxyhydrazines, **1**, could facilitate the use of this reaction for synthetic purposes.

## Theoretical Details

The smallest compound studied experimentally for the thermal decomposition of **1** was $R^1{=}CH_3$ and $R^2{=}(CH_2)_2CH_3$. The simplest system used in this study was $R^1{=}R^2{=}H$ (**a**). All geometries for system **a** were fully optimized for the species in pathway III at the Hartree−Fock (HF),[5] Møller−Plesset second-order perturbation (MP2)[6] and density functional theory (DFT),[7] with the Becke3 hybrid exchange functional and the Perdew86 correlation functional (B3P86),[8] levels of theory. Previous theoretical work has shown that the B3P86 functional gives similar,[9] and sometimes superior,[10] results to the B3LYP functional. To test the ability of **a** to accurately represent the experimental compound, two larger systems were optimized with density functional theory: **b** ($R^1{=}CH_3$ and $R^2{=}H$) and **c** ($R^1{=}R^2{=}CH_3$), where **c** is the closest representation of the smallest experimental compound studied ($R^1{=}CH_3$ and $R^2{=}(CH_2)_2CH_3$). All calculations were performed with the Gaussian 94 (G94)[11] suite of programs using the basis set 6-31G**.[12] To achieve accurate energetics and compare the methodologies, the following single-point energies for **a** were calculated: MP2//HF, MP3//MP2, MP4//MP2, CCSD//HF, CCSD//MP2, CCSD//B3P86, CCSD(T)//HF, CCSD(T)//MP2, and CCSD(T)//B3P86, where CCSD is coupled cluster singles and doubles and CCSD(T) is CCSD with perturbative triples.[13] For **b**, the CCSD//B3P86 and CCSD(T)//B3P86 single-point energies were calculated. For **c**, CCSD//B3P86 and CCSD(T)//B3P86 single-point energies were only calculated for the intermediate, **3c**, second transition state, **4c**, and the products, **5c** and **6c**. Reaction path I was investigated at the HF and B3P86 levels with **a** in the basis set 6-31G**. Frequency calculations at the HF, MP2, and B3P86 levels of theory were performed to obtain zero-point energies and frequencies for all species in reaction paths I and III for **a**. Frequency calculations at the DFT level of theory were performed for **b** and **c**.

## Results and Discussion

**System a, Pathway III, B3P86.** The B3P86 optimized geometries of system **a** ($R^1{=}R^2{=}H$), for all relevant species involved in reaction path III can be found in Figure 1 and their corresponding energetics in Table 1. A total of nine isomers were investigated for the reactant, **1a**. There are five possible isomers due to rotation about the N−N $\sigma$ bond and inversion at the nitrogens. The lowest energy structure of these five isomers was the $C_2$ symmetry gauche structure shown in Figure 1, **1a**. The $C_2$ symmetry gauche structure has four isomers due to rotations about the N−C and N−O $\sigma$ bonds and of these four isomers, the lowest energy structure was found to be the structure shown in Figure 1, **1a**. The C═O bond is longer and the C−N bond is shorter than expected due to a resonance contribution shown in Figure 2.

The optimized geometry of the first transition state (TS), **2a**, is shown in Figure 1. This is a central (as opposed to an early or late) transition state, which is evident by a 0.49 Å shortening of the C−O bond distance (2.35 Å → 1.86 Å) that will shorten an additional 0.52 Å to become the C−O bond in the product, **6a** (1.34 Å). The N−N bond is also intermediate between that in **1a** and **3a**. There is a significant lengthening (0.42 Å) of the N−O bond distance of the leaving group. The rest of the molecule is planar and looks very similar to the intermediate, **3a**. There is a shortening of the C═O bond and a lengthening

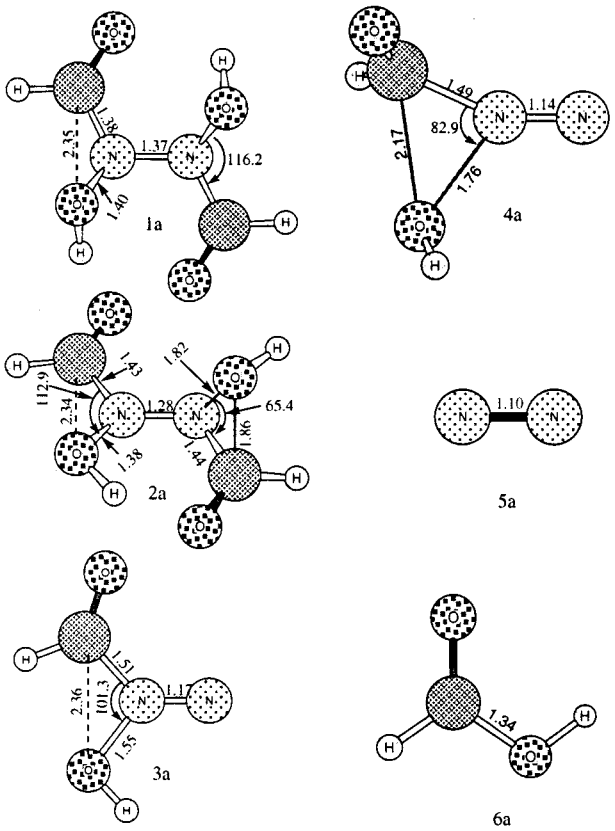


**Figure 1.** Model **a** geometry optimization results at the B3P86 level for the reactant, **1a**; first transition state, **2a**; intermediate, **3a**; second transition state, **4a;** and the products, **5a** and **6a**, in reaction path III.

**TABLE 1: Energetics (kcal/mol) for Reaction Path III with System a**

| | **1a** | **2a** | **3a**+**6a** | **4a**+**6a** | **5a**+2(**6a**) |
|---|---|---|---|---|---|
| B3P86//B3P86[a] | 0.00 | 23.76 | −3.51 | −0.54 | −100.6 |
| CCSD//B3P86[a] | 0.00 | 30.89 | −11.27 | −6.37 | −120.1 |
| CCSD(T)//B3P86[a] | 0.00 | 24.95 | −12.98 | −10.78 | −116.8 |
| | **1a′** | **2a′** | **3a′**+**6a** | **4a**+**6a** | **5a**+2(**6a**) |
| HF//HF[b] | 0.00 | 47.94 | −13.34 | 6.10 | −137.9 |
| MP2//HF[b] | 0.00 | 25.16 | −5.75 | −14.23 | −124.8 |
| MP2//MP2[c] | 0.00 | 23.21 | −8.80 | −13.20 | −127.0 |
| MP3//MP2[c] | 0.00 | 35.07 | −2.50 | 3.39 | −120.9 |
| MP4//MP2[c] | 0.00 | 20.33 | −10.41 | −12.61 | −123.7 |
| CCSD//HF[b] | 0.00 | 32.13 | −9.10 | −4.92 | −124.4 |
| CCSD//MP2[c] | 0.00 | 31.93 | −7.17 | −1.42 | −123.5 |
| CCSD(T)//HF[b] | | | 0.00 | 0.40 | −112.4 |
| CCSD(T)//MP2[c] | | | 0.00 | 2.97 | −111.7 |

[a] B3P86 zero-point energy (ZPE) and thermal corrections included. [b] HF ZPE and thermal corrections included. [c] MP2 ZPE and thermal corrections included.

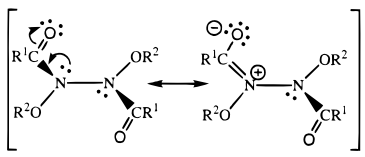

**Figure 2.** Resonance structure contributed to the lengthening of the C═O bond and the shortening of the C−N bond in the reactant, **1**.

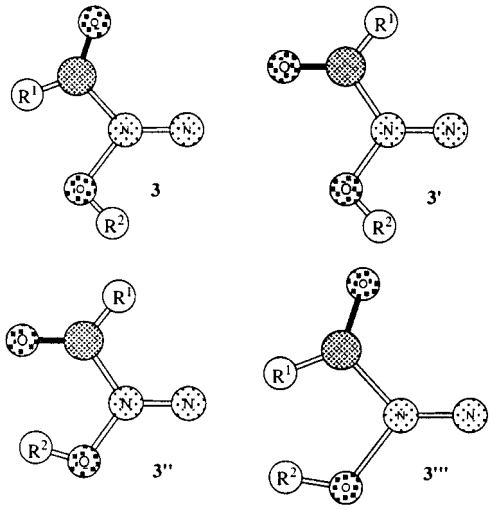


**Figure 3.** Possible structures for the intermediate, **3**, in reaction path III. Model **a**, R═R′═H; model **b**, R═H and R′═$CH_3$; and model **c**, R═R′═$CH_3$.

of the C−N bond distance of the groups that remain in the intermediate, due to loss of resonance with the lone pair on the nitrogen (Figure 2). A frequency calculation on **2a** gave one imaginary frequency (326.0*i* $cm^{-1}$) whose normal coordinate appears to correspond to the migration of the OH group to the carbon of the COH group attached to the same nitrogen and a rotation about the N−OH and N−COH $\sigma$ bonds. The first TS barrier at the CCSD(T)//B3P86 is 24.9 kcal/mol which is only 1.2 kcal/mol higher in energy than the B3P86//B3P86 energy. The CCSD//B3P86 barrier is 30.9 kcal/mol so, the addition of perturbative triples lowered the barrier by 5.9 kcal/mol.

The four possible conformations (**3**, **3′**, **3″**, **3‴**) for the intermediate are shown in Figure 3 and at the B3P86 level, **3a** was found to be the lowest energy structure, and the reaction to this point is exothermic by 13.0 kcal/mol at the CCSD(T)// B3P86 level. There is further shortening of the C═O bond and an increase in the N−C bond due to the complete loss of resonance (Figure 2). The intermediate is planar to allow for the delocalization of the $\pi$ electrons on the O, C and N atoms. It is interesting to note that the N−N bond distance in the intermediate, **3a**, is shorter (1.16 Å) than would be expected for a N−N double bond (1.21 Å).

This phenomenon was investigated by the geometry optimization of three simple model systems, dimethylnitrene, acylmethylnitrene, and hydroxymethylnitrene at the B3P86 level of theory with the basis set 6-31G**. It was found that the N−N bond distance was 1.21 Å for dimethylnitrene and acylmethylnitrene but decreased to 1.17 Å for hydroxymethylnitrene. A natural bond order analysis (NBO)[14] was also performed on dimethylnitrene and hydroxymethylnitrene. The NBO results show that dimethylnitrene has the expected $sp^2$ hybridization on both nitrogen atoms with a typical double bond and two lone pairs on the unsubstituted nitrogen. The NBO analysis on hydroxymethylnitrene shows a complex mixing of the orbitals. There are three formal N−N bonds: a strong $\sigma$ bond, a strong $\pi$ bond between the $p_z$ orbitals, and a weak $\pi$ bond. There is only one lone pair on the unsubstituted nitrogen in an sp like hybridized orbital. In addition, the "$\sigma$" bond between the nitrogen and the oxygen (N−OH) is mostly centered on the oxygen (72% O and 28% N). Therefore, the OH substituent has a fair amount of ionic character, which would explain the significant lengthening (0.17 Å) of the N−OH bond distance from **1a** to **3a**.

The second TS geometry, **4a**, is shown in Figure 1. Compound **4a** is a very early transition state with a decrease in the C−OH bond of only 0.19 Å. There is a lengthening of the C═O bond, due to resonance, as the product is being formed. A frequency calculation on **4a** resulted in one imaginary frequency (176.9*i* $cm^{-1}$) whose normal coordinate appears to correspond to rotations around the N−OH and N−C $\sigma$ bonds. Because of the small imaginary frequency and the possibility that these rotations would lead to another conformation of the intermediate species instead of the products, an intrinsic reaction coordinate (IRC) calculation was performed. The IRC calculation confirmed that **4a** goes to the products, **5a** and **6a**, in the forward direction and goes to the intermediate **3a** in the reverse direction. The barrier for the second TS is very small, 2.2 kcal/mol at the CCSD(T)//B3P86 level. The exothermicity of the first step is 13.0 kcal/mol at the CCSD(T)//B3P86 level which is 10.8 kcal/mol greater than the second TS barrier. Therefore, even in solution where much of the excess energy could be dissipated, one would expect rapid reaction to the products. The very small second barrier explains why experimentalists have been unable to trap the intermediate nitrene.

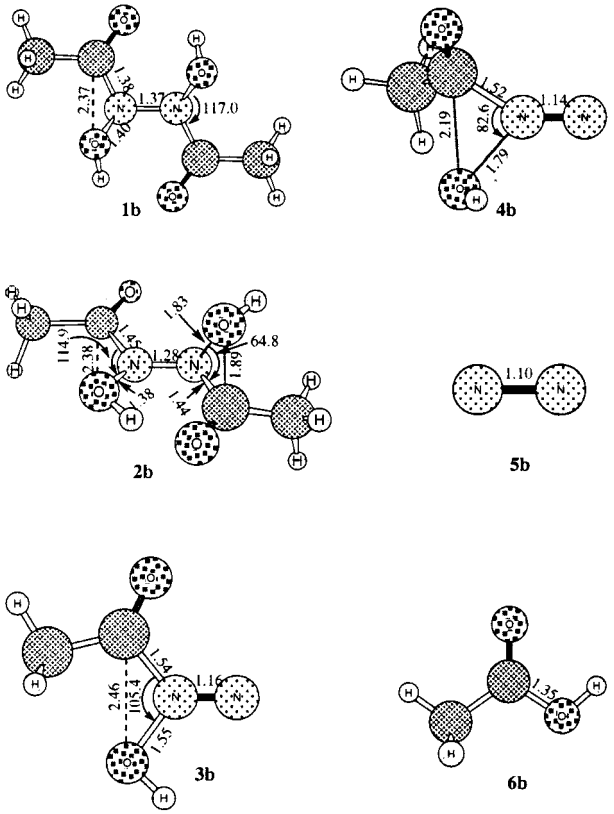


**Figure 4.** Model **b** geometry optimization results at the B3P86 level for the reactant, **1b**; first transition state, **2b**; intermediate, **3b**; second transition state, **4b**; and the products, **5b** and **6b**, in reaction path III.

The products, **5a** and **6a**, are shown in Figure 1 and the B3P86 calculations reproduce the experimental bond distances of 1.10 Å for the N−N bond[15] and 1.34 Å for the C−OH bond distance in formic acid.[16] Overall, this very exothermic reaction (−116.8 kcal/mol at the CCSD(T)//B3P86 level) is consistent with the complete decomposition of **1** occurring under mild conditions.

**System b and c, Pathway III, B3P86.** Systems **b** ($R^1$═$CH_3$, $R^2$═H) and **c** ($R^1$═$R^2$═$CH_3$) were investigated to determine how increasing the size of the system effects the reaction. The B3P86 optimized geometry for systems **b** and **c** can be found in Figures 4 and 5, respectively, and their corresponding energetics are given in Table 3. There is very little difference between the geometry of the reactants for the three systems (**a, b**, and **c**). The steric interaction of the bulkier methyl group in **1b** increased

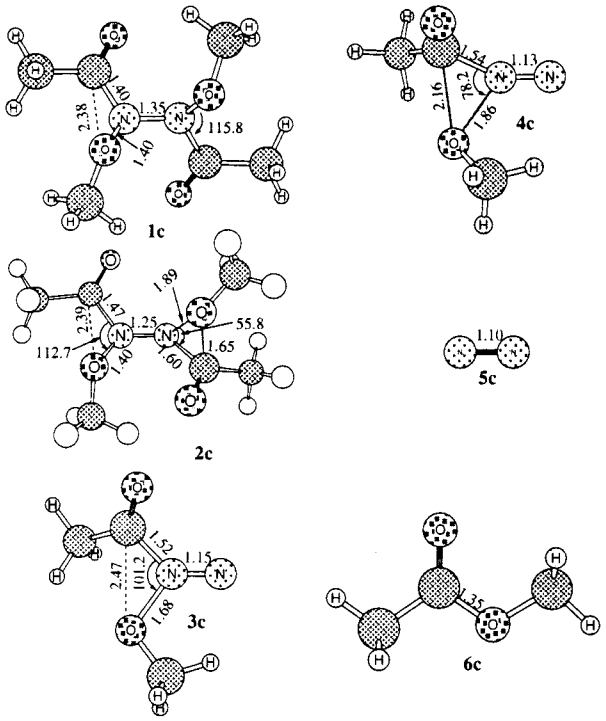


**Figure 5.** Model **c** geometry optimization results at the B3P86 level for the reactant, **1c**; first transition state, **2c**; intermediate, **3c**; second transition state, **4c**; and products, **5c** and **6c**; in reaction path III.

**TABLE 2: Transition State Barriers (kcal/mol) for Reaction Path III with System a**

| | barrier 1 | barrier 2 |
|---|---|---|
| B3P86//B3P86[a] | 23.76 | 2.97 |
| CCSD//B3P86[a] | 30.89 | 4.90 |
| CCSD(T)//B3P86[a] | 24.95 | 2.20 |
| HF//HF[b] | 47.94 | 19.44 |
| MP2//HF[b] | 25.16 | −8.48 |
| MP2//MP2[c] | 23.21 | −4.40 |
| MP3//MP2[c] | 35.07 | 5.89 |
| MP4//MP2[c] | 20.33 | −2.20 |
| CCSD//HF[b] | 32.13 | 4.18 |
| CCSD//MP2[c] | 31.93 | 5.74 |
| CCSD(T)//HF[b] | | 0.40 |
| CCSD(T)//MP2[c] | | 2.97 |

[a] B3P86 ZPE and thermal corrections included. [b] HF ZPE and thermal corrections included. [c] MP2 ZPE and thermal corrections included.

the C−N−O angle by 0.8° and increased the C···OH nonbonding distance by 0.02 Å compared to **1a**. The addition of another methyl group **1c**, causes a decrease in the C−N−O angle by 0.4 Å due to steric interation with the $OCH_3$ group attached to the same nitrogen and an increase in the C···OH nonbonding distance by 0.03 Å compared to **1a**. There is also a 0.02 Å increase in the N−$COCH_3$ bond distance which is accompanied by a 0.02 Å decrease in the N−N bond distance.

The first TS, **2**, is also a central transition state for system **b**, with a 0.48 Å shortening of the C−O bond distance that will shorten another 0.54 Å to become the C−O bond in the product **6b** (1.35 Å), but it is a slightly later transition state for system **c** with a 0.73 Å shortening of the C−O bond distance that will only have to shorten another 0.30 Å to become the C−O bond in the product **6c** (1.35). Once again, there is a significant lengthening (0.43 Å, **b**; 0.49 Å, **c**) of the N−$OR^2$ bond distance of the leaving group and the N−N bond is intermediate between that in **1** and **3**. There is a lengthening of the C═O bond and a shortening of the C−N bond of the groups remaining attached in the intermediate due to loss of resonance (Figure 2) and the

**TABLE 3: Energetics (kcal/mol) for Reaction Path III with Systems b and c[b]**

| | $\Delta E^a$ B3P86// B3P86 | $\Delta E^a$ CCSD// B3P86 | $\Delta E^a$ CCSD(T)// B3P86 | $\Delta H°$ B3P86// B3P86 | $\Delta G°$ B3P86// B3P86 |
|---|---|---|---|---|---|
| **1b** | 0.00 | 0.00 | 0.00 | 0.00 | 0.00 |
| **2b** | 23.43 | 29.85 | 23.81 | 23.43 | 24.15 |
| **3b+6b** | −4.86 | −11.63 | −13.12 | −4.27 | −20.17 |
| **4b+6b** | −2.23 | −8.12 | −12.18 | −1.64 | −15.53 |
| **5b+2(6b)** | −100.5 | −119.7 | −115.7 | −99.27 | −123.6 |
| **1c** | 0.00 | | | 0.00 | 0.00 |
| **2c** | 34.71 | | | 34.71 | 36.64 |
| **3c+6c** | −13.43 | 0.00 | 0.00 | −12.83 | −26.29 |
| **4c+6c** | −10.83 | 4.00 | 2.42 | −10.24 | −22.80 |
| **5c+2(6c)** | −103.7 | −102.7 | −95.41 | −102.5 | −126.0 |
| barrier 2 | | | | | |
| **3b-4b** | 2.63 | 3.51 | 0.94 | 2.63 | 4.64 |
| **3c-4c** | 2.60 | 4.00 | 2.42 | 2.60 | 3.48 |

[a] B3P86 ZPE and thermal corrections included. [b] CCSD and CCSD(T) single-point energy calculations were not performed on **1c** and **2c** due to the large system size.

TS becomes planar in system **b** but not in system **c** where the $OCH_3$ group is unable to achieve planarity due to steric hinderence. A frequency calculation on **2b** and **2c** gave one imaginary frequency (341.0*i* $cm^{-1}$, 335.4*i* $cm^{-1}$) whose normal coordinate, again, appears to correspond to a migration of the OH to the $COCH_3$ group with rotations about the N−OH and N−$COCH_3$ $\sigma$ bonds. The first TS barrier for system **b** was 23.8 kcal/mol at the CCSD(T)//B3P86 level which is only 1.1 kcal/mol lower than the barrier calculated for system **a** at the same level of theory. Again, the CCSD(T)//B3P86 barrier is very similar to the B3P86//B3P86 barrier (1.7 kcal/mol difference). The first TS barrier for system **c** was 34.7 kcal/mol at the B3P86//B3P86 level of theory, which is 11.3 kcal/mol higher in energy than the B3P86//B3P86 barrier for system **b**.

For the intermediate, **3**, there is a 0.1 Å difference between the C···O nonbonding distance of **3a** (2.36 Å) and that of **3b** (2.46 Å) and **3c** (2.47 Å). The C−N bond distance in **3** varies by 0.03 Å or less in the three systems (**a**, **b**, and **c**). The O−N bond distance increases by 0.13 Å from **3b** (1.55 Å) to **3c** (1.68 Å). In system **c**, the intermediate, **3c**, is no longer planar. The $COCH_3$ group rotates out of the plane due to steric hindrance but the $OCH_3$ remains in the plane to accommodate the delocalization of the $\pi$ electrons over the O−N−N atoms. The exothermicity of the reaction to this point (**1**→**3**) is −4.9 kcal/mol at the B3P86//B3P86 level and −13.1 kcal/mol at the CCSD(T)//B3P86 level for system **b** and −13.4 kcal/mol at the B3P86//B3P86 level for system **c**.

The geometries for the second TSs, **4b** and **4c**, have all of the characteristics of the second TS for system **a**, **4a**. The second barrier for system **b** did decrease to 1.1 kcal/mol at the CCSD(T)//B3P86 level from 2.2 kcal/mol for system **a** but increased to 2.4 kcal/mol for system **c**. The second TS appears to have a flat potential energy surface with respect to the rotation of the substituents. Systems **b** and **c** also had a small imaginary frequency for **4b** (194.1*i* $cm^{-1}$) and **4c** (207.3*i* $cm^{-1}$) whose normal coordinates appears to correspond to rotations about the N−C and N−O $\sigma$ bonds. Although we did not again perform an IRC calculation from the TSs, **4b** and **4c**, the normal coordinate mode was very similar to that found for **4a**. It is interesting to note that for systems **a** and **b** the N−C bond distance shows an unexpected decrease by 0.02 Å in the second TSs, **4a** and **4b**, compared to the intermediates, **3a** and **3b**, but for system **c** the N−C bond distance increases by 0.02 Å.

The products, **6b** and **6c**, are planar and show a lengthening of the C═O bond distance due to resonance contributions.

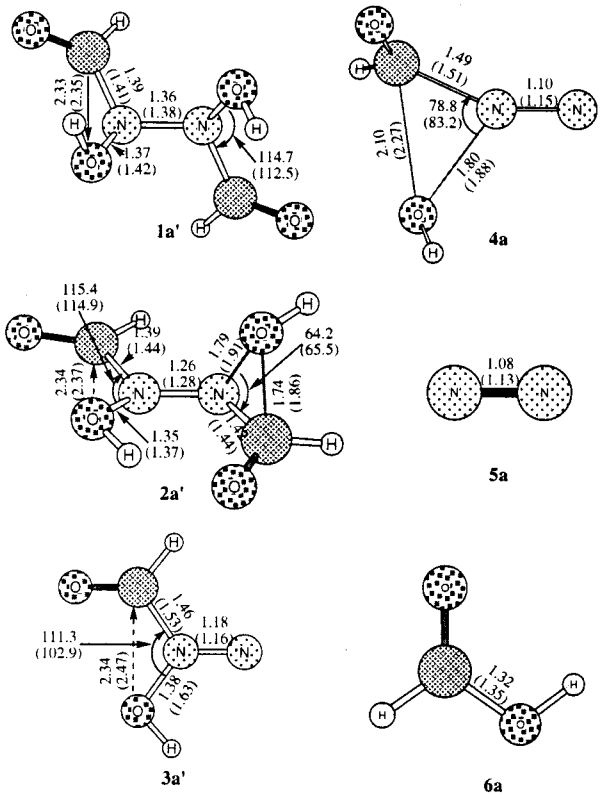


**Figure 6.** Model **a** geometry optimization results at the HF and (MP2) levels for the reactant, **1a′**; first transition state, **2a′**; intermediate, **3a′**; second transition state, **4a**; and the products, **5a** and **6a** in reaction path III. The second transition state, **4a**, is lower in energy than the intermediate, **3a′**.

**TABLE 4: Absolute Energies (au) for the Reactant and the Intermediate for Reaction Path III and System a**

| | 1a | 3a |
|---|---|---|
| CCSD//B3P86 | −487.6310 | −298.3626 |
| CCSD//HF | −487.6248 | −298.3562 |
| CCSD//MP2 | −487.6310 | −298.3577 |
| CCSD(T)//B3P86 | | −298.3966 |
| CCSD(T)//HF | | −298.3863 |
| CCSD(T)//MP2 | | −298.3938 |

Again, this is a very exothermic reaction with $\Delta H° \approx -100$ kcal/mol (Table 3). The Gibbs free energy, given in Table 3, for systems **b** and **c** are both large and negative ($\Delta G° \approx -120$ kcal/mol) which is in agreement with the experimental observation that the reaction occurs spontaneously.

**System a, Pathway III, HF and MP2.** The HF and MP2 optimized geometries of system **a** for all relevant species involved in reaction path III can be found in Figure 6 and their corresponding energetics in Table 1. A comparison of the results for HF and MP2 geometries with those for B3P86 shows that the HF and MP2 geometries for **1a′**, **2a′**, and **3a′** have a slightly different conformation than their B3P86 counterparts **1a**, **2a**, and **3a**. In the lowest energy structure for the reactant, **1a′**, at the HF and MP2 levels of theory, both the COH and OH groups are rotated approximately 180° about the N−O and N−C $\sigma$ bonds from the lowest energy conformer at the B3P86 level. The absolute CCSD single-point energies for **1a′** (HF and MP2) and **1a** (B3P86) can be found in Table 4. For the reactant, the CCSD//B3P86 energy is 3.9 kcal/mol lower in energy than the CCSD//HF energy and less than 0.1 kcal/mol lower in energy than the CCSD//MP2 energy.

The first TS at the HF and MP2 level, **2a′**, looks very similar to **2a** (B3P86) for the leaving group but the conformation of the COH group remaining attached to the nitrogen still maintains an approximately 180° rotation about the N−C $\sigma$ bond from the lowest energy conformer at the B3P86 level. Although these geometries are somewhat different, the HF and MP2 energetics for the first barrier look very similar to the B3P86 energetics (Table 1).

The lowest energy conformer for the intermediate at the HF and MP2 levels of theory is **3′**, shown in Figure 3 and Figure 6 (**3a′**). The HF and MP2 intermediates, **3a′**, differ from the B3P86 intermediate, **3a**, by a 180° rotation about the N−C bond. The CCSD and CCSD(T) single-point energies for **3a′** (HF and MP2) and **3a** can also be found in Table 4. The CCSD//B3P86 energy is 6.9 kcal/mol lower in energy than the CCSD//HF energy and 2.9 kcal/mol lower in energy than the CCSD//MP2 energy. The CCSD(T)//B3P86 energy is 9.4 kcal/mol lower in energy than the CCSD(T)//HF energy and 1.6 kcal/mol lower in energy than the CCSD//MP2 energy. The fact that the B3P86 lowest energy conformation has the lowest CCSD(T) single-point energy indicates that it is the correct conformation, although the difference in energy is very small.

The geometries for the second TS, **4a**, are very similar to that found at the B3P86 level and the normal coordinate of the imaginary frequency for the HF and MP2 second TSs are very similar to the normal coordinate found for the B3P86 imaginary frequency (488.7*i* cm$^{-1}$, HF; 216.3*i* cm$^{-1}$, MP2). Unexpectedly, a negative barrier for the second step in the reaction path at the MP2//HF, MP2//MP2, and MP4//MP2 levels was found, with and without the ZPE and thermal corrections. An intrinsic reaction coordinate (IRC) calculation was performed on the HF and MP2 optimized **4a** TSs, and they went to the products in both the forward and reverse directions. Since the second TS is very early, the step size in the reverse direction was decreased and the convergence criteria was tightened in an attempt to find the intermediate, **3a′**. The IRC calculation was unable to find the intermediate in the reverse direction. At this point, we suspected that there was a serious failure in the HF and MP2 representation of the potential energy surface for this reaction.

The negative barrier for the second TS and the inability of the IRC calculation to "find" the intermediate required further investigation. To determine whether the problem was in the theory, basis set, or the size of the system, a number of tests were performed with varying basis set size and system size. At the basis set size 6-31G**, for system **a** the structure labeled **3′** in Figure 3 was found to be the lowest energy structure at the HF and MP2 level (**3a′** in Figure 6). **3a″** was found to be higher in energy than **3a′** by 1.6 and 3.4 kcal/mol at the HF and MP2 levels, respectively. **3a** is 2.1 kcal/mol higher in energy than **3a′** at the HF level and is not a minimum at the MP2 level. **3a‴** is not a minimum at the HF or MP2 level. Since there is such a small difference between the energy levels of the B3P86 intermediate, **3a**, and the HF minimum **3a′**, calculations were performed with a larger basis set to determine whether the energetics would change. The basis set was increased to Dunning's correlation consistent triple-$\zeta$ with polarization (cc-pvtz)[17] basis set (4s, 3p, 2d, 1f) for system **a** and the **3a′** confomer was still found to be lower in energy than **3a** by 2.5 kcal/mol therefore, the basis set size is not a factor. Systems **b** and **c** were investigated for all conformations shown in Figure 3 at the HF and MP2 levels of theory with the 6-31G** basis set. For systems **b** and **c**, HF still found **3′** to be the lowest energy structure, while for MP2 the lowest energy conformations were **3b′** and **3c**. Therefore, for this system, HF calculations fail to describe the reaction properly regardless of basis set size or system size and only for system **c** are the MP2 and B3P86

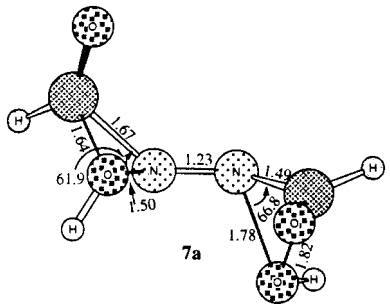


**Figure 7.** Model **a** geometry optimization result from AM1 parameters by the MOPAC program in the CAChe modeling system for the concerted "transition state", **7a**, in reaction path I.

conformer for **3** the same. It is possible that MP2 would describe the reaction properly with system **c** but the computational cost would be high compared to B3P86.

The products, **5a** and **6a**, are shown in Figure 6. The N−N bond distance is 0.02 Å shorter than the experimental value (1.10 Å) at the HF level and 0.03 Å longer than the experimental value at the MP2 level. This is consistent with the lack of correlation at the HF level and an overestimation of correlation effects at the MP2 level. The C−OH bond distance in formic acid, **6a**, is 0.02 Å shorter than the experimental value at the HF level and 0.01 Å longer than the experimental value at the MP2 level. The overall exothermicity of the reaction is again very similar to the exothermicity at the B3P86 level.

**System a, Pathway I, HF and B3P86.** All attempts to converge a transition state calculation for the concerted elimination (pathway I) TS reverted to the two step 1,1-elimination TS, **2a**. The geometry for the concerted elimination TS obtained by semiempirical AM1 parametrized[4] calculations (Figure 7) was used for a frequency calculation at the HF and B3P86 levels. Two imaginary frequencies were found at the HF level (780.4*i* and 563.9*i* $cm^{-1}$) and B3P86 level (524.4*i* and 326.3*i* $cm^{-1}$) with a barrier of 139.2 and 88.4 kcal/mol, respectively. Therefore, the concerted elimination "transition state" is a second-order saddle point on the potential energy surface where both imaginary frequencies lead to the two step 1,1-elimination TS, **2a**.

## Conclusions

Density functional calculations showed that the decomposition of *N*,*N*′-diacyl-*N*,*N*′-dialkoxyhydrazines proceeds via a two step 1,1-elimination (pathway III) and not via a concerted elimination (pathway I). The critical point on the concerted elimination pathway is a second-order saddle point that is 64 kcal/mol higher in energy than the first TS barrier in the 1,1-elimination at the B3P86//B3P86 level. For the 1,1-elimination, the B3P86 calculations find a $C_2$ symmetry, gauche structure for the reactant **1**, and a central first TS, **2**, with a barrier of 24 kcal/mol at the CCSD(T)//B3P86 level for models **a** and **b** and a barrier of 35 kcal/mol at the B3P86//B3P86 level for model **c**. The intermediate, **3**, lies approximately 13 kcal lower in energy than the reactant **1**. The second TS, **4**, is very early and is only 1−3 kcal/mol higher in energy than the intermediate. The exothermicity of the first step coupled with the very low second barrier explains why experimentalists were unable to trap any intermediate nitrenes. The overall reaction is very exothermic ($\Delta H°$ (B3P86//B3P86) $\approx -100$ kcal/mol) and spontaneous ($\Delta G°$ (B3P86//B3P86) $\approx -120$ kcal/mol), which is consistent with the reaction completing under mild conditions.

We looked at a number of different systems and found that increasing the system size, replacing H with $CH_3$ for $R^1$, had very little effect on the energetics of this reaction but replacing H with $CH_3$ for $R^2$ caused an 11 kcal/mol increase in the first transition state barrier. A 34 kcal/mol barrier for the rate-determining step is still a reasonable value for the experimental reaction conditions (12 h at 25 °C for $R^1$=*t*-Bu and $R^2$=$CH_3$). An early kinetic study[3] on the thermal decomposition of N−N′-diacetyl-*N*,*N*′-dipropoxyhydrazine ($R^1$=$CH_3$, $R^2$=$(CH_2)_2CH_3$) in bromoform found very little temperature dependence on the rate of reaction and an activation barrier of only 5 kcal/mol, a result very different from ours. A kinetic study of the thermal decomposition of neat *N*,*N*′-diacyl-*N*,*N*′-dialkoxy hydrazines would be useful in clarifying this discrepancy. This study also shows that both HF and MP2 theory fail to describe properly all aspects of this reaction mechanism even in larger basis sets. For this system, density functional theory B3P86 seems to give better geometries than HF or MP2 and its energetics are very similar to the CCSD(T)//B3P86 energetics.

**Acknowledgment.** We thank The Welch Foundation (A-648) and the National Science Foundation (CHE-9800184) for their generous support. We would also like to thank the Supercomputing Facility at Texas A&M University for computer time.

## References and Notes

(1) De Almeida, M. V.; Barton, D. H. R.; Bytheway, I.; Ferreira, A. J.; Hall, M. B.; Liu, W.; Taylor, D. K.; Thomson, L. *J. Am. Chem. Soc.* **1995**, *117*, 4870.

(2) a) Barton D. H. R.; Girijavallabhan, M.; Sammes, P. G. J. *Chem. Soc., Perkin. Trans. 1* **1977**, 929−932. (b) de Oliveira Baptista, M. J. V.; Barrett, A. G. M.; Barton, D. H. R.; Girijavallaghan, M.; Jennings, R. C.; Kelly, J.; Papadimitriou, V. J.; Turner, J. V.; Usher, N. A. *J. Chem. Soc., Perkin Trans. 1* **1977**, 1477.

(3) Cooley, J. H.; Mosher, M. W.; Khan, M. A. *J. Am. Chem. Soc.* **1968**, *90*, 1867.

(4) a) Dewar, M. J. S.; Zoebisch, E. G.; Healy, E. F.; Stewart, J. J. P. *J. Am. Chem. Soc.* **1985**, *107*, 3902. (b) Stewart, J. J. P. *The MOPAC Manual*; Pittsburgh Supercomputing Center: Pittsburgh, PA. (c) *CAChe User's Guide*; Tektronix, Inc: Beaverton, OR.

(5) Roothaan, C. C. *J. Rev. Mod. Phys.* **1960**, *32*, 179.

(6) a) Møller, C.; Plesset M. S. *Phys. Rev.* **1936**, *46*, 618. (b) Pople, J. A.; Binkley, J. S.; Seeger, R. *Int. J. Quantum Chem.* **1976**, *S10*, 1.

(7) Parr, R. G.; Yang, W. *Density-Functional Theory of Atoms and Molecules*; Oxford University Press: Oxford, 1989.

(8) a) Becke, A. D.; *Phys. Rev. A.* **1988**, *38*, 3098. (b) Perdew, J. P. *Phys. Rev. B* **1992**, *45*, 13244.

(9) Zaric, S.; Hall, M. B. *Molecular Modeling and Dynamics of Bioinorganic Systems 3. High Technology*; Kluwer Academic Publishers: Dordrecht, 1997; Vol. 41, p 255.

(10) (a) Neumann, R.; Nobes, R. H.; Handy, N. C. *Mol. Phy.* **1996**, *87*, 1. (b) Wilberg, K. B.; Stratmann, R. E.; Frisch, M. J. *Chem. Phys. Lett.* **1998**, *297*, 60. (c) Arulmozhiraha, S.; Kolandaivel, P.; Ohashi, O. *J. Phys. Chem.* **1999**, *103*, 3073.

(11) Frisch, M. J.; Trucks, G. W.; Schlegel, H. B.; Gill, P. M. W.; Johnson, B. G.; Robb, M. A.; Cheeseman, J. R.; Keith, T.; Petersson, G. A.; Montgomery, J. A.; Raghavachari, K.; Al-Laham, M. A.; Zakrzewski, V. G.; Ortiz, J. V.; Foresman, J. B.; Cioslowski, J.; Stefanov, B. B.; Nanayakkara, A.; Challacombe, M.; Peng, C. Y.; Ayala, P. Y.; Chen, W.; Wong, M. W.; Andres, J. L.; Replogle, E. S.; Gomperts, R.; Martin, R. L.; Fox, D. J.; Binkley, J. S.; Defrees, D. J.; Baker, J.; Stewart, J. P.; Head-Gordon, M.; Gonzalez, C. *Gaussian 94*, Revision D.4*;* Gaussian, Inc.: Pittsburgh, PA, 1995.

(12) a) Ditchfield, R.; Hehre, W. J.; Pople, J. A. *J. Chem. Phys.* **1971**, *54*, 724. (b) Hehre, W. J.; Ditchfield, R.; Pople, J. A. *J. Chem. Phys.* **1972**, *56*, 209. (c) Hariharan, P. C.; Pople, J. A. *Mol. Phys.* **1974**, *27*, 209. (d) Gordon, M. S. *Chem. Phys. Lett.* **1980**, *76*, 163. (e) Hariharan, P. C.; Pople, J. A. *Theor. Chim. Acta* **1973**, *28*, 213. (f) Frisch, M. J.; Pople, J. A.; Binkley, J. S. *J. Chem. Phys.* **1984**, *80*, 3265.

(13) Bartlett, R. H. *Annu. Rev. Phys. Chem.* **1981**, *32*, 359.

(14) Weinhold, F. *Natural Bond Orbital Analysis Programs, Revision 4.0*, Board of Regents of the University of Wisconsin System on behalf of the Theoretical Chemistry Institute: Madison, WI, 1996.

(15) Gray, D. E., Ed. *American Insitute of Physics Handbook*; McGraw-Hill: New York, 1972.

(16) Streitwieser, A., Jr.; Heathcock, C.H. *Introduction to Organic Chemistry*; Macmillan Publishing Company: New York, 1985.

(17) Dunning, T. H., Jr. *J. Chem. Phys.* **1989**, *90*, 1007.